Monolithic Fabrication of Metal-Free On-Paper Self-Charging Power Systems

Yingchun Su, Han Xue, Yujie Fu, Shiqian Chen, Zheng Li, Lengwan Li, Ainars Knoks, Olga Bogdanova, Pēteris Lesničenoks, Roberts Palmbahs, Mika-Matti Laurila, Matti Mäntysalo, Mattias Hammar, Anders Hallén, Nils Nordell, and Jiantong Li*

Self-charging power systems (SCPSs) are envisioned as promising solutions for emerging electronics to mitigate the increasing global concern about battery waste. However, present SCPSs suffer from large form factors, unscalable fabrication, and material complexity. Herein, a type of highly stable, eco-friendly conductive inks based on poly(3,4-ethylenedioxythiophene) :poly(styrenesulfonate) (PEDOT:PSS) are developed for direct ink writing of multiple components in the SCPSs, including electrodes for miniaturized spacer-free triboelectric nanogenerators (TENGs) and microsupercapacitors (MSCs), and interconnects. The principle of "one ink, multiple functions" enables to almost fully print the entire SCPSs on the same paper substrate in a monolithic manner without post-integration. The monolithic fabrication significantly improves the upscaling capability for manufacturing and reduces the form factor of the entire SCPSs (a small footprint area of ≈2 cm × 3 cm and thickness of ≈1 mm). After pressing/releasing the TENGs for ≈79000 cycles, the 3-cell series-connected MSC array can be charged to 1.6 V while the 6-cell array to 3.0 V. On-paper SCPSs are promising to serve as lightweight, thin, sustainable, and low-cost power supplies.

1. Introduction

The rapid development of emerging electronics (such as wearable electronics, the Internet of Things, and soft robotics) imposes the demand for efficient, lightweight, flexible, and portable power sources.[1,2] Currently widely-used batteries are considered ineffective due to their bulky form factor and heavy weight, their need for frequent recharging/replacement and critical raw materials (such as Li and Co), and the increasing global concern of battery waste. Recently, self-charging power systems (SCPSs) have been envisioned as promising alternatives for emerging electronics.[1,3] The SCPSs integrate energy harvesters, power management, and energy storage devices to convert environmental energy into electricity and regulate and store the electricity to form a self-charging, stable, and maintenance-free power supply for electronics.[3,4] Great progress has been achieved in developing various SCPSs to harvest energy from different types of sources, including light, temperature, and mechanical motion.[1] However, the research fields are still confronting many challenges. It is difficult to integrate energy harvesters with energy storage devices in a compact manner as mostly reported SCPSs are usually formed by two separately fabricated units (usually using different processes) through manual post-integration,[5] which will cause large form factors and poor scalability of the SCPSs. Most emerging electronics, especially wearable and implantable electronics, require compact, lightweight, and biocompatible power sources. Also, since many emerging electronics are designed for one-time use, low cost, scalable fabrication, and eco-friendliness are highly desired characteristics of the power sources. At

Y. Su, H. Xue, Y. Fu, S. Chen, Z. Li, M. Hammar, A. Hallén, N. Nordell, J. Li
School of Electrical Engineering and Computer Science
KTH Royal Institute of Technology
Electrum 229, Kista 16440, Sweden
E-mail: jiantong@kth.se

L. Li
Department of Fibre and Polymer Technology
Wallenberg Wood Science Center
KTH Royal Institute of Technology
Stockholm 10044, Sweden

A. Knoks, O. Bogdanova, P. Lesničenoks, R. Palmbahs
Institute of Solid State Physics
University of Latvia
Riga LV-1063, Latvia

M.-M. Laurila, M. Mäntysalo
Faculty of Information Technology and Communication Sciences
Tampere University
Tampere 33720, Finland

ADVANCED
SCIENCE NEWS

www.advancedsciencenews.com

ADVANCED
FUNCTIONAL
MATERIALS

www.afm-journal.de
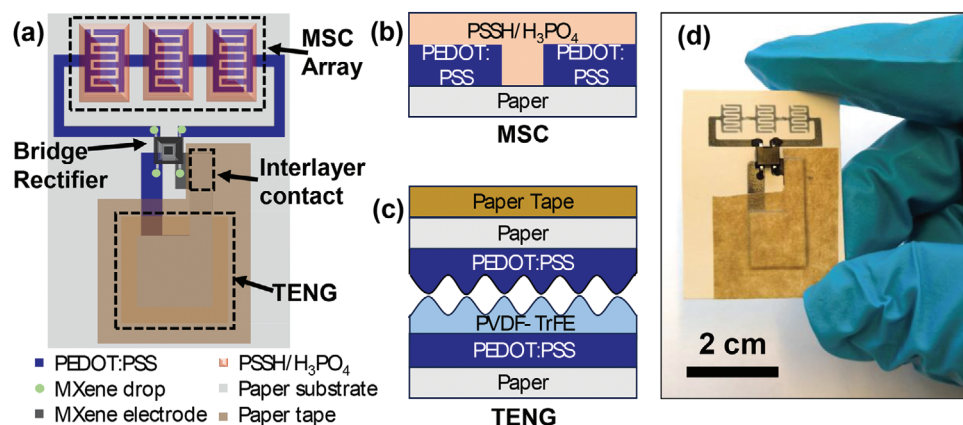
Figure 1. On-paper SCPSs. a–c) Schematic of a) the entire SCPS, b) the MSC device structure, and c) the TENG device structure. d) Photograph of a monolithically fabricated on-paper SCPS.

present, it is very challenging to fabricate SCPSs to meet all the requirements.[1,2]
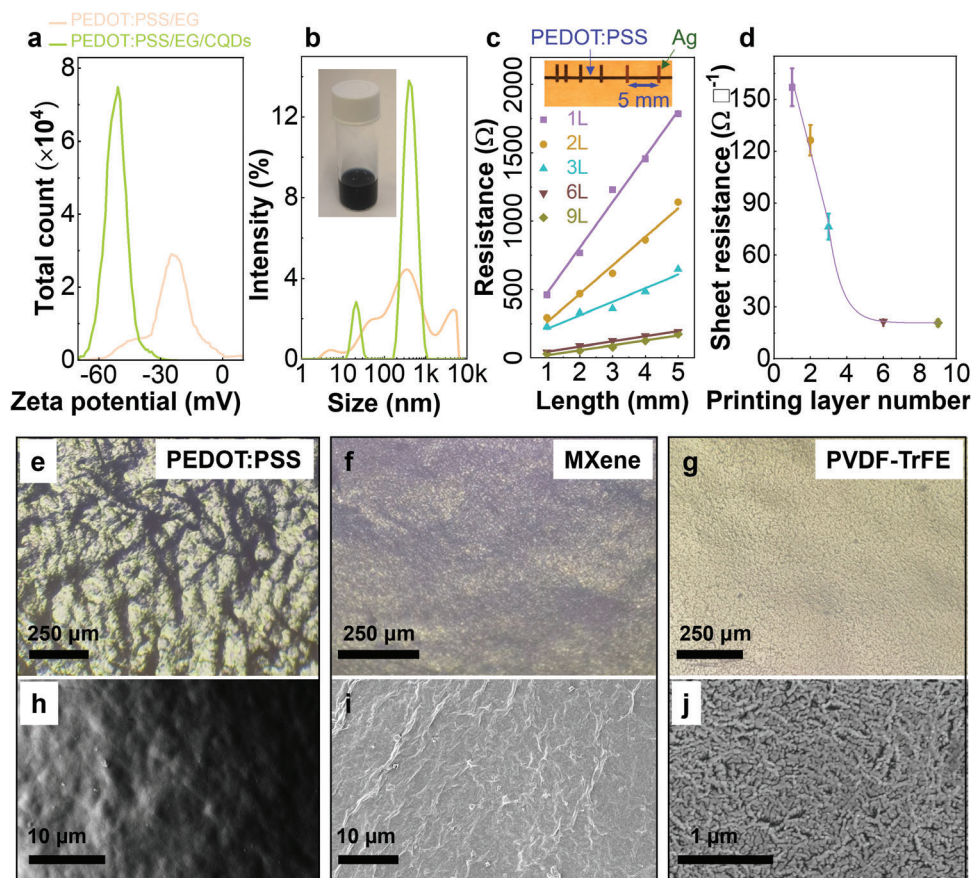
Containing the required energy harvesting and storage devices, and the optional power management, the fabrication of SCPSs often relies on a large variety of materials and processes. From the perspective of materials, most SCPSs need noble metals (such as Au and Ag) or toxic metals[6-10] as the electrodes (or current collectors) and interconnects, and multiple types of active materials to realize functionality in the different components. Some SCPSs use expensive, or even toxic active materials to improve the key performance,[11] which greatly increases the fabrication complexity and cost, and reduces the sustainability.[2] Based on the present fabrication techniques, it is challenging to get compact SCPS, even just to miniaturize some individual components, such as triboelectric nanogenerators (TENGs).[12,13]

To overcome the abovementioned flaws of the present SCPSs, in this work, we have developed a facile, scalable, low-cost, and nearly monolithic process to fabricate compact (footprint area ≈2 cm × 3 cm), thin (<1 mm thickness in most area) and metal-free SCPSs on paper substrates. The key is to develop a single type of organic (metal-free) inks to directly print highly conductive patterns on paper substrates to simultaneously act as the electrodes for the energy harvesting devices (TENGs) and energy storage devices (microsupercapacitors, MSCs), as well as interconnects for the whole systems. In particular, the combination between the large surface roughness of the paper substrates and the outstanding conformability of PEDOT:PSS produces highly rough electrodes to provide a simple route to miniaturize the TENGs with a spacer-free structure. The principle of "one ink, multiple functions" enables us to almost fully print the entire SCPSs in a monolithic manner, and hence avoid the need for "post-integration". Remarkably, the metal-free on-paper SCPSs have been able to convert mechanical force, applied through a linear motor, to electricity and charge the MSCs up to 3.0 V for six MSC cells connected in series.

2. Results and Discussion

As shown in **Figure** 1a, our on-paper SCPS comprises an MSC array, a TENG, and a full-wave bridge rectifier. The all-solid-state

MSCs are based on interdigitated electrodes of conducting polymer poly(3,4-ethylenedioxythiophene):poly(styrenesulfonate) (PEDOT:PSS) submerged in the gel electrolyte of poly(4-styrenesulfonic acid)/phosphoric acid (PSSH/H_3PO_4) composite (Figure 1b). The TENG works in the vertical contact-separation mode[14,15] and is constituted of three components: a lower electrode of stacked poly(vinylidene fluoride-trifluoroethylene) (PVDF-TrFE)/PEDOT:PSS/paper structure, an upper electrode of stacked PEDOT:PSS/paper structure, and a paper tape to cover and fix the two electrodes (Figure 1a,c). Similar to the previous study on all-plastic TENGs,[16] in our TENGs the PEDOT:PSS layer in the upper electrode plays the role of "triboelectric electrode". Because in addition to the general role of the electrode, it also acts as one of the triboelectric layers. The simple assembly with paper tape can vertically stack the two electrodes to form the complete TENGs. Despite the lack of spacer between the two triboelectric layers (PEDOT:PSS in the upper electrode and PVDF-TrFE in the lower electrode), our on-paper TENGs can still work in the contact-separation mode.[14] The enabling factor could be ascribed to the highly rough surface of the on-paper PEDOT:PSS electrode, as discussed in the next section. TENG will generate charges at the surfaces of the triboelectric layers and hence instantaneous (pulsed) voltage and current with reverse polarity in the circuits.[14] A commercial bridge rectifier is then used to convert the alternating current (AC) output to direct current (DC) before storing it in the MSCs to form stable power sources for later use. Because our printed PEDOT:PSS patterns are of low sheet resistance on paper substrates, they also serve as interconnects for all three key components (MSCs, TENG, and rectifier). However, for the "interlayer contacts" between the TENG upper electrode and the interconnect on the lower paper substrate (Figure 1a), PEDOT:PSS is not effective due to their large contact resistance (≈1.5 MΩ cm², Table S1, Supporting Information). Nevertheless, we have found that MXene (Ti$_3$C$_2$T$_x$) is an excellent material for interlayer contacts due to the significantly lower contact resistance (≈5.1 Ω cm², Table S1, Supporting Information). So MXene was printed as an interface on both the bottom paper substrate and the upper PEDOT:PSS electrode surface (Figure S1, Supporting Information; Figure 6a) to improve the interlayer contacts. The contacts between the PEDOT:PSS (or MXene) interconnects and the rectifier pins

ADVANCED
SCIENCE NEWS

www.advancedsciencenews.com

ADVANCED
FUNCTIONAL
MATERIALS

www.afm-journal.de

Figure 2. Characterization of the inks used to print the SCPSs. a) Zeta potential and b) Dynamic laser scattering (DLS) particle size distribution of the diluted PEDOT:PSS inks without and with CQDs, (inset, b) Photograph of the PEDOT:PSS/EG/CQD ink. c) Length-dependent resistance of the DIW-printed PEDOT:PSS lines on the paper substrate for various numbers of printing layers, (inset) Photograph of a DIW-printed PEDOT:PSS line equipped with inkjet printed silver contacts. d) Dependence of sheet resistance on the number of printing layers for the on-paper PEDOT:PSS electrodes (sample size $n = 3$). e–g) Optical micrographs and h–j) SEM images of the DIW-printed e,h) PEDOT:PSS, f,i) MXene, and g,j) PVDF-TrFE patterns on paper substrates.

are simply realized through a small drop of highly conductive MXene ink.

As a result, almost the entire SCPSs are made of the common material PEDOT:PSS. Only three local regions need different materials (PSSH/H_3PO_4 for MSC electrolyte, PVDF-TrFE for one of the triboelectric layers of the TENG, and MXene for interlayer contacts). This makes it feasible for us to develop a nearly full printing process to fabricate compact on-paper SCPSs (as shown in Figure 1d) in a monolithic manner. In the following sections, we will introduce in sequence the inks, the full printing processes of the key components (MSCs and TENG), and the monolithic printing of the entire SCPSs.

2.1. Highly Conductive Organic Inks

The key to our SCPSs is the formulation of highly conductive PEDOT:PSS ink. The pristine PEDOT:PSS is actually of low conductivity ≈1 S cm^{-1},[17,18] while ethylene glycol (EG) is an excellent dopant and can increase the conductivity of PEDOT:PSS by one order of magnitude (Figure S2a, Supporting Information).

The effects of EG on the conductivity and capacitance of PEDOT:PSS electrodes are shown in Figure S2 (Supporting Information). However, the PEDOT:PSS/EG (volume ratio of 8:2) dispersion is not stable with a low zeta potential of −23 ± 3 mV, large particle size, and high polydispersity (**Figure 2a,b**). Previously, we have reported that the simultaneous addition of two materials, electrochemically exfoliated graphene and graphene quantum dots, can significantly stabilize the PEDOT:PSS/EG dispersion.[19] In this work, we have also found that the addition of a very small amount (0.15 mg mL^{-1}, ≈1.7 wt.% of PEDOT:PSS, Table S2, Supporting Information) of carbon quantum dots (CQDs) can effectively stabilize the PEDOT:PSS/EG dispersion with a more negative zeta potential of −52.1 ± 0.8 mV (a zeta potential of absolute value ≥ 60 mV corresponds to excellent stability[19]), as well as smaller particle size and lower polydispersity (Figure 2b). Due to their small size (<20 nm, Figure S3, Supporting Information), the CQDs can easily attach to the PEDOT:PSS chains. Their rich hydrophilic amine (N–H) and hydroxyl (O–H) groups[20] significantly increase the hydrophilicity of PEDOT:PSS and hence its stability in water-based ink. The use of only one single type of stabilizing material (CQDs) greatly simplifies the ink formulation. The stable PEDOT:PSS ink enables

ADVANCED
SCIENCE NEWS

www.advancedsciencenews.com

ADVANCED
FUNCTIONAL
MATERIALS

www.afm-journal.de

direct and reliable printing of highly conductive patterns on paper substrates through the direct ink writing (DIW) technique.[21] The transmission line method (TLM, Figure 2c,d) is used to estimate the sheet resistance of the printed PEDOT:PSS lines on paper substrates. One single printing layer can produce a low sheet resistance of 157 ± 11 Ω $\square^{-1}$. The sheet resistance reduces to 76 ± 8 Ω $\square^{-1}$ for 3 layers and 21.7 ± 0.8 Ω $\square^{-1}$ for 6 layers. The low sheet resistance of the printed PEDOT:PSS patterns and the flexibility of the DIW process allow us to develop a monolithic process to print the entire SCPSs on paper substrates.

In this work, we have also found one crucially important feature of our PEDOT:PSS ink that is very beneficial for SCPSs. The ink solvent EG can wash away the coatings of some commercial paper substrates (such as the Korsnäs white paperboard used in this work) and expose the pulp. Similar to our previous study,[22] the printed PEDOT:PSS conforms to the exposed pulp surface (Figure 2e,h) to form very rough conductive electrodes. As for the MSCs, the rough PEDOT:PSS electrodes provide a large surface area to increase the areal capacitance. However, when it comes to the interlayer contacts, the effective contact area between two rough PEDOT:PSS electrodes is significantly decreased, leading to extremely large interlayer contact resistance (≈ 1.5 MΩ cm^2). Nevertheless, the MXene inks (only with water as the solvent) can form a smooth surface on the paper substrate (Figure 2f,i). The smooth surface greatly increases the effective contact area between two MXene electrodes and reduces the contact resistance by 6 orders of magnitude (to ≈ 5.1 Ω cm^2). However, the contact resistance between one MXene electrode and one PEDOT:PSS electrode is still as high as ≈ 0.2 MΩ cm^2, suggesting that the effective contact area between the rough PEDOT:PSS layer and the smooth MXene layer is still very small.
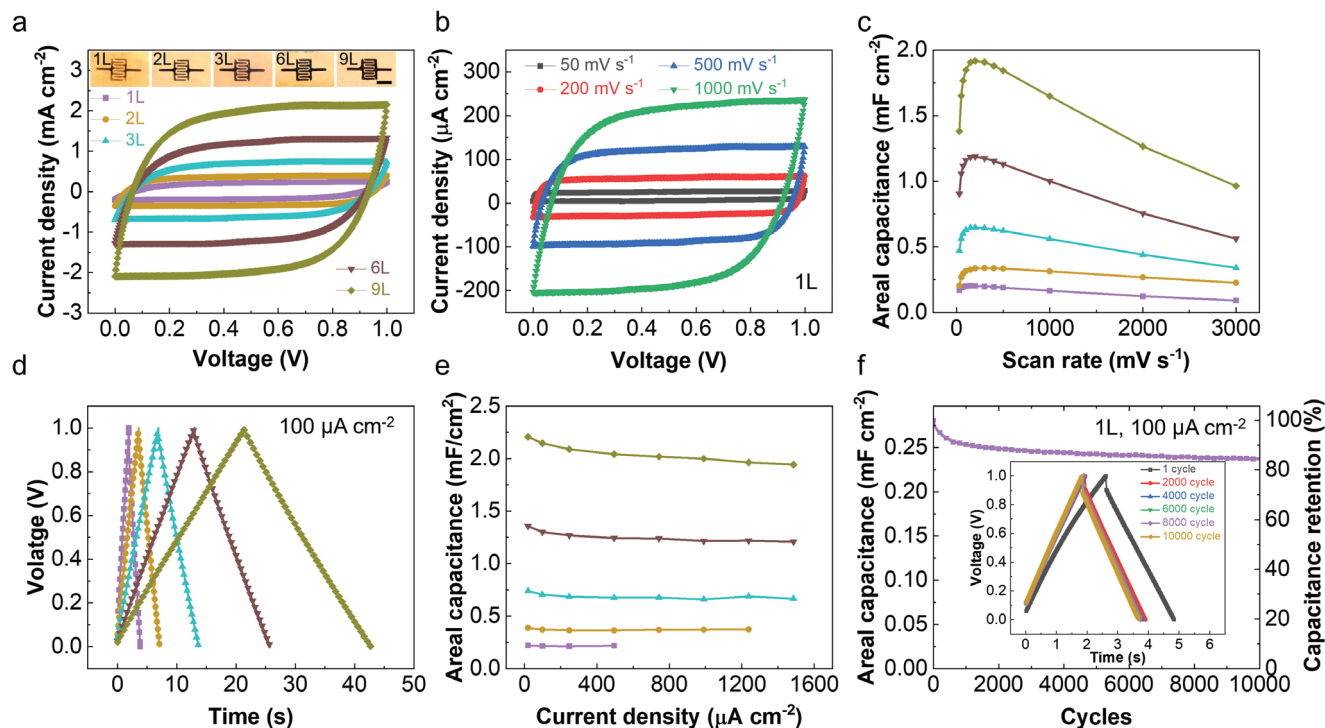
This finding could explain the working mechanism of our spacer-free TENGs. Initially, when the rough PEDOT:PSS layer contacts the PVDF-TrFE layer (Figure 2g,j), the effective contact area is very small (similar to the case of PEDOT:PSS/MXene interlayer contact). But under pressure, the microstructure in the rough PEDOT:PSS layer may deform significantly to greatly increase the effective contact area with the PVDF-TrFE layer and finally improve output electricity.[23–25] Therefore, the press and release of the TENGs can generate a large difference in the effective contact area between the two triboelectric layers, even without any spacer. The spacer-free structure of our on-paper TENGs greatly reduces the fabrication complexity and improves the compactness of the entire SCPSs.

2.2. Fully Printed Individual Microsupercapacitors (MSCs) and MSC Arrays

The MSCs are fabricated through DIW printing of the PEDOT:PSS ink to produce the interdigitated electrodes with various printing layers, followed by drop casting of the PSSH/H_3PO_4 electrolytes to bridge the electrodes. Hereafter, "nL" is used to denote an electrode made from n printing layers/passes of the PEDOT:PSS ink. The fingers in the MSC electrodes are ≈ 3 mm long, 300–500 µm wide, and interspaced with a gap of 200–300 µm (inset, **Figure 3a**). The footprint area (including the inter-finger gaps) of each MSC is ≈ 24 mm^2. The cyclic voltammetry (CV) test for the 1L-MSCs (Figure 3b) exhibits excellent capacitive behavior with nearly perfect rectangular CV curves at all the scan rates ranging from 50 to 1000 mV s^{-1}. With increasing the number of printing layers from 1 to 9, all the MSCs still exhibit excellent capacitive behavior at the high scan rate of 1000 mV s^{-1} with a nearly perfect rectangular shape (Figure 3a). However, consistent with our previous work,[19] the areal capacitance of our MSCs exhibits non-monotonic dependence on the scan rate (Figure 3c): the areal capacitance increases with scan rate when scan rate <200 mV s^{-1}, and decreases when the scan rate >200 mV s^{-1}. The reason/mechanism has not been clear but is likely related to the addition of EG (Figure S2b, Supporting Information) and/or CQDs.[19] The symmetrical and triangular galvanostatic charge-discharge (GCD) curves in Figure 3d confirm the excellent capacitive behavior of the on-paper MSCs. The areal capacitance extracted from the GCD curves (Figure 3e) is almost independent of the current density and increases from ≈ 0.22 mF cm^{-2} for the 1L MSCs to ≈ 2 mF cm^{-2} for the 9L MSCs. After 10000 GCD cycles at a current density of 100 µA cm^{-2}, the 1L MSC retains 84% of the initial capacitance (Figure 3f). The good scalability of the areal capacitance with electrode thickness (printing layers) of the MSCs facilitates their integration into the SCPSs, while their high-rate capability (up to 1000 mV s^{-1}) and long cycle life ensure their efficiency to quickly store the instantaneous (pulsed) electricity from the TENGs in a long term.

In general, the output voltage of a TENG is higher than the working voltage window of an MSC. It is therefore desired to connect multiple MSCs in series to increase the working voltage window to match the output voltage of the TENG. Our conductive PEDOT:PSS ink also allows the direct writing of multiple MSCs connected in series on paper substrates to produce metal-free 1 L MSC arrays (**Figure 4a**). The MSC arrays can be charged at the high scan rate of 1000 mV s^{-1} with ideally rectangular CV curves (Figure 4b), and meanwhile, the working voltage window increases proportionally to 3 V for the 3-series-cell (3S) MSC arrays and 6 V for 6-series-cell (6S) MSC arrays. All MSC arrays show triangular GCD curves at the current of 24 µA (Figure 4c). With the same charging current and time, the one-cell, 3S, and 6S MSC arrays reach the voltage of 1, 3, and 6 V, respectively. They are also fully discharged at approximately the same time under the same discharging current. These suggest the excellent scalability of the MSC arrays. The only shortcoming is that the voltage drop at the start of discharging (i.e., IR drop) increases with increasing the cell number (Figure 4c), mainly because of the increased resistance caused by the series connection, as confirmed by the equivalent series resistance measured from electrochemical impedance spectroscopy (EIS) of the MSC arrays with different cell numbers (Figure S4, Supporting Information). This work has also validated the effect of series connections in MSC arrays. With increasing the cell number, not only does the working voltage window of the MSC arrays increase, but also their rate capability increases proportionally. As shown in Figure 4d, the single-cell MSC can be charged at 1000 mV s^{-1} with excellent rectangular CV curves, but when the scan rate is over 3000 mV s^{-1}, the CV curves become lens-like. In contrast, the 3S array retains excellent CV curves at 3000 mV s^{-1} (Figure 4e) while the 6S

ADVANCED
SCIENCE NEWS
www.advancedsciencenews.com

ADVANCED
**FUNCTIONAL**
MATERIALS
www.afm-journal.de

Figure 3. Electrochemical characterization of the printed on-paper MSCs with various number of printing layers ranging from 1 to 9. a) CV curves at 1000 mV s^{-1}, (inset) Photograph of the MSCs (scale bar: 4 mm). b) CV curves for the 1L MSC at different scan rates. c) Areal capacitance extracted from the CV curves against scan rate. d) GCD curves at a current density of 100 μA cm^{-2}. e) Areal capacitance extracted from the GCD curves against current density. f) Areal capacitance and capacitance retention of a 1L MSC for 10 000 GCD cycles at 100 μA cm^{-2}, (inset) GCD curves after different number of cycles.

array can maintain the proper CV characteristics, even at 6000 mV s^{-1} (Figure 4f). To collect the fast-changing, instantaneous output electricity from TENG, the 3S and 6S exhibited more competitive performance than that of a one-cell device. We also explore the cycling performance of the MSC arrays at a high scan rate. After 10 000 CV cycles at 1000 mV s^{-1} for one cell (Figure 4g), 3000 mV s^{-1} for the 3S array (Figure 4h), and 6000 mV s^{-1} for the 6S array (Figure 4i), respectively, all the MSC arrays retain 81–86% of the initial capacitance. The increased rate capability and retained cycle life suggest the advantage of MSC arrays over individual MSCs in storing the instantaneous output electricity from the TENGs.

2.3. Fully Printed Triboelectric Nanogenerators (TENGs)

Figure 5a illustrates the fabrication process of our printed TENGs. First, the pairs (upper and lower) of PEDOT:PSS electrodes, consisting of the 1.1 cm × 1.1 cm charge collecting part and 0.3 cm × 3 cm extending part for external connection, or interconnect, are printed on paper substrates. The PVDF-TrFE film (1.6 cm×1.6 cm) is printed on the square charge collecting part of the lower electrodes. The thickness of PEDOT:PSS electrode and PVDF-TrFE film is ≈53 ± 4 and 35 ± 5 μm, respectively, measured by a KOSLO digital thickness gauge. After the PVDF-TrFE film dries, the upper electrodes are cut out, flipped, and attached to the lower electrodes with the square charge col-

lecting parts aligned to each other. Finally, paper tape is used to fix the two electrodes and finish the assembly of the TENGs. The working principle of spacer-free TENG was described in Supporting Information (Figure S5, Supporting Information). To characterize their output performance, the TENGs are pressed by a linear motor with controllable force and frequency. As shown in Figure 5, every press/release of the TENGs simultaneously generates pulsed voltage and current. To confirm that the electric output comes from the TENG (not from instrumental, or environmental noise), the polarity of the TENGs is switched to test their output voltage both in the forward and reverse connection modes (Figure 5i). The reverse output voltage signal with the same amplitude in the two connection directions validates the generation of electric output from the triboelectric effect of the TENG device.[26,27] To test if the piezoelectric effect contributes to the TENG performance, a traditional piezoelectric energy device of stacked Ag/PVDF-TrFE/PEDOT:PSS/paper structure was fabricated, where the Ag electrode was directly pasted on the PVDF-TrFE layer to avoid the triboelectric effect. The device only attained an output voltage of <1 V, and the forward and reverse connection did not change the polarity of the output signal (Figure S6, Supporting Information). Thus, in this work, the TENG performance is dominated by the triboelectric effect. In agreement with previous studies,[23-25,28,29] the output voltage (with a load resistance of 300 MΩ) and short-circuit current of our TENGs both increase with the applied force (Figure 5b–d) and frequency (Figure 5f–h). The maximum peak-to-peak voltage is ≈12 V and the maximum peak-to-peak current is ≈60 nA at the force of
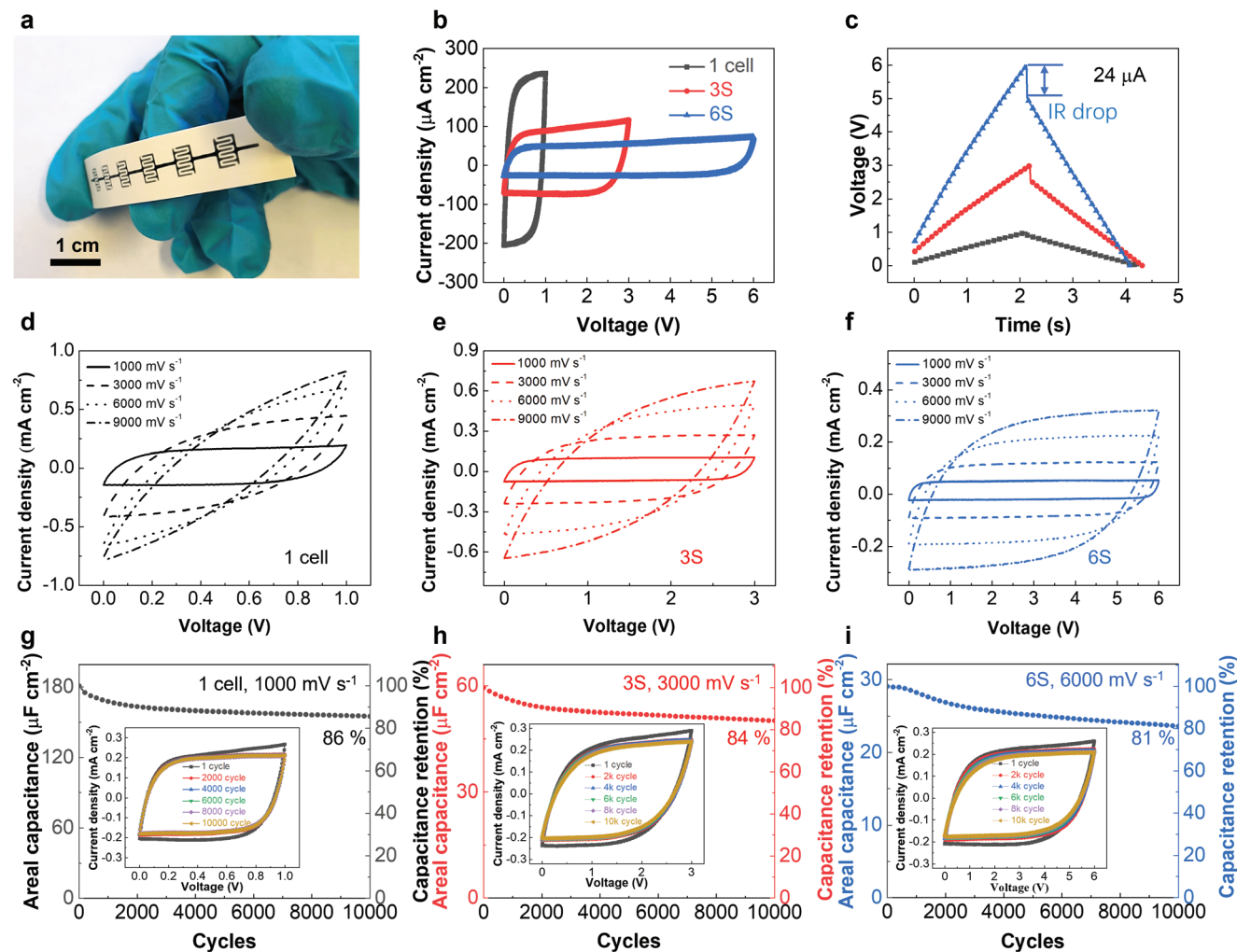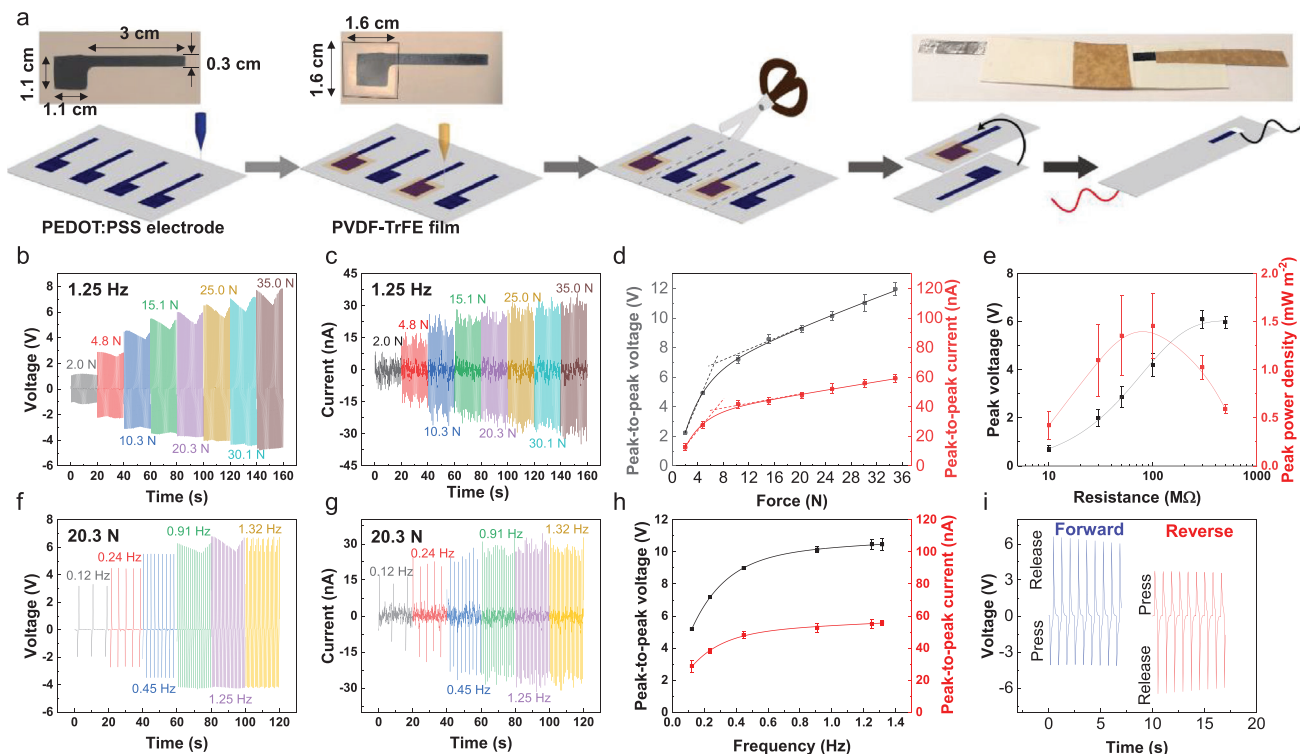
Figure 4. Electrochemical characterization of the printed on-paper 1L MSC arrays. a) Photograph of the 6S array. b) CV curves at 1000 mV s^{-1} and c) GCD curves at 24 µA of the MSC arrays. d–f) CV curves at scan rates ranging from 1000 to 9000 mV s^{-1} of the d) 1-cell, e) 3S, and f) 6S arrays. g–i) Cycling performance for 10000 CV cycles at scan rate of g) 1000 mV s^{-1} for 1 cell, h) 3000 mV s^{-1} for 3S, and i) 6000 mV s^{-1} for 6S arrays, (insets) CV curves at different number of cycles.

≈35 N (corresponding to a pressure of ≈446 kPa) and frequency of ≈1.3 Hz. In addition, both the peak-to-peak voltage and current (Figure 5d) exhibit different increase rates at two distinct force regions since the electric output of the TENGs is determined by the real contact area:[23] at low force (<7 N) region, the increase is much faster than that in the high force (>7 N) region. It should be ascribed to the pressure (force)-dependent contact area between the rough surfaces.[23-25] In the low-pressure region, the effective contact area increases with the pressure due to the deformation of interfacial microstructure, [24,25] such as the rough morphology of our on-paper PEDOT:PSS electrodes, while at the high-pressure region the contact area saturates.[23] Aiming to evaluate the maximum output power, various load resistances ranging from 10 to 500 MΩ are connected in series with the TENGs. The peak power density is calculated by the square of the average peak voltage divided by the resistance and device area.[30,31] With a load resistance of 50 – 100 MΩ, a maximum peak power density of ≈1.5 mW m^{-2} is achieved (Figure 5e).

2.4. Monolithic Fabrication of the Entire Self-Charging Power Systems (SCPSs)

Using the merit of "one ink, multiple functions", we have developed a monolithic process to fabricate the entire on-paper SCPSs without any post-integration (**Figure 6**a). The fabrication is almost fully based on the DIW process. Only four types of ink materials (PEDOT:PSS, PVDF-TrFE, MXene, and PSSH/H$_3$PO$_4$) are used in the fabrication, together with a commercial bridge rectifier chip to convert the AC output of the TENG to DC electricity to charge the MSCs. The rectifier is the only non-printable component in our SCPSs, but our monolithic process makes it easy to integrate a small-size rectifier chip into the SCPSs to retain the system compactness. The rectifier can be recycled and reused while all the other components are fully based on eco-friendly materials.

Most of the components in the SCPSs are printed with the PEDOT:PSS inks. As illustrated in Figure 6a, on a common paper

**ADVANCED
SCIENCE NEWS**

www.advancedsciencenews.com

**ADVANCED
FUNCTIONAL
MATERIALS**

www.afm-journal.de

Figure 5. Characterization of the fully printed TENGs. a) Schematic of the fabrication process. b) Output voltage (with a load resistance of 300 MΩ) and c) short-circuit current of one TENG under different forces (frequency 1.25 Hz). d) Dependence of average peak-to-peak voltage and current on the applied force (sample size $n \geq 10$). e) Average peak voltage and power as functions of a series of load resistance (sample size $n \geq 12$). f) Output voltage (with 300 MΩ load resistance) and g) short-circuit current of one TENG under the same force of 20.3 N but with different frequencies. h) Dependence of average peak-to-peak voltage and current on the frequency of the applied force (sample size $n \geq 3$). i) Output voltage (with 300 MΩ load resistance) in the forward and reverse connection modes.

substrate, first, the PEDOT:PSS ink is used to print the electrodes for the MSC array, the upper and lower TENG electrodes, and the interconnect. Benefitting from the direct patterning merit of the DIW process, the cell number in the MSC array can be readily adjusted. In this work, we printed 3S (Figure 1d) with a capacitance of 14.3 µF and 6S MSC array (Figure S7, Supporting Information) with a capacitance of 7.0 µF to match the output voltage of ≈6 V from the TENG. Then, the PVDF-TrFE ink and the MXene ink are used to print the triboelectric layer on the lower electrode of the TENG and the interlayer contacts, respectively. Afterward, the bridge rectifier chip is mounted with its main body fixed by a double-sided tape, and its pins connect the interconnect through drop-cast MXene ink. Next, the TENG is assembled simply by cutting away the upper electrode, flipping and aligning it to the lower electrode, and fixing the two electrodes with paper tape. Finally, the PSSH/H$_3$PO$_4$ gel electrolytes are drop-cast onto the MSC electrodes to complete the fabrication of the entire SCPSs.

In the SCPSs, when a cyclic press-release force (21.6 N and 1.52 Hz, Figure 6b) is applied to the TENG, an AC output voltage (with a load resistance of 300 MΩ) is generated and turns to DC voltage after being regulated by the bridge rectifier (Figure 6c). The electricity generation is highly stable and durable, with only a slight decline (3.16%) of the peak-to-peak voltage after 12 000 cycles (Figure 6d). This merit may result from the excellent mechanical stability of the PEDOT:PSS paper electrodes, and en-

ables the continuous charging of the MSC arrays in the long term. As shown in Figure 6e, the electricity generated by the TENG can effectively charge up the 1L MSC arrays. At the same charging time of 14.5 h (or ≈79 000 press-release cycles of the TENG), a 3S MSC array can be charged up to 1.6 V and a 6S array up to 3.0 V. This value has already approached the highest voltage attained in other recently reported SCPCs (Table S3, Supporting Information).[7-10,32-35] Importantly our SCPCs also possess the advantages of using metal-free materials, eco-friendly paper substrate, and an easy-operation DIW method. The characteristic of the charging curves is consistent with other studies:[34,36] the voltage at first increases linearly (quickly) with charging time and then becomes saturated. Considering the charging time of 3 h in the linear region, the 3S and 6S arrays are charged to 0.95 and 1.77 V, respectively. The attained voltage is nearly proportional to the cell number in the MSC arrays, suggesting that when charged by the TENGs, the MSC arrays exhibit similar scalability to the case of GCD tests (Figure 4c). This also implies that with the same charging time, the 6S array can store almost twice as much energy as the 3S array, according to $E = 1/2CV^2$ with the capacitance C reversely proportional and the voltage V proportional to the cell number. As a demo for powering electronics in practical application, after being charged by the TENG for ≈20 h, the 3S array can supply the display of a digital timer (Video S1, Supporting Information). As the power from our 3S MSCs and TENG is ≈30 µW
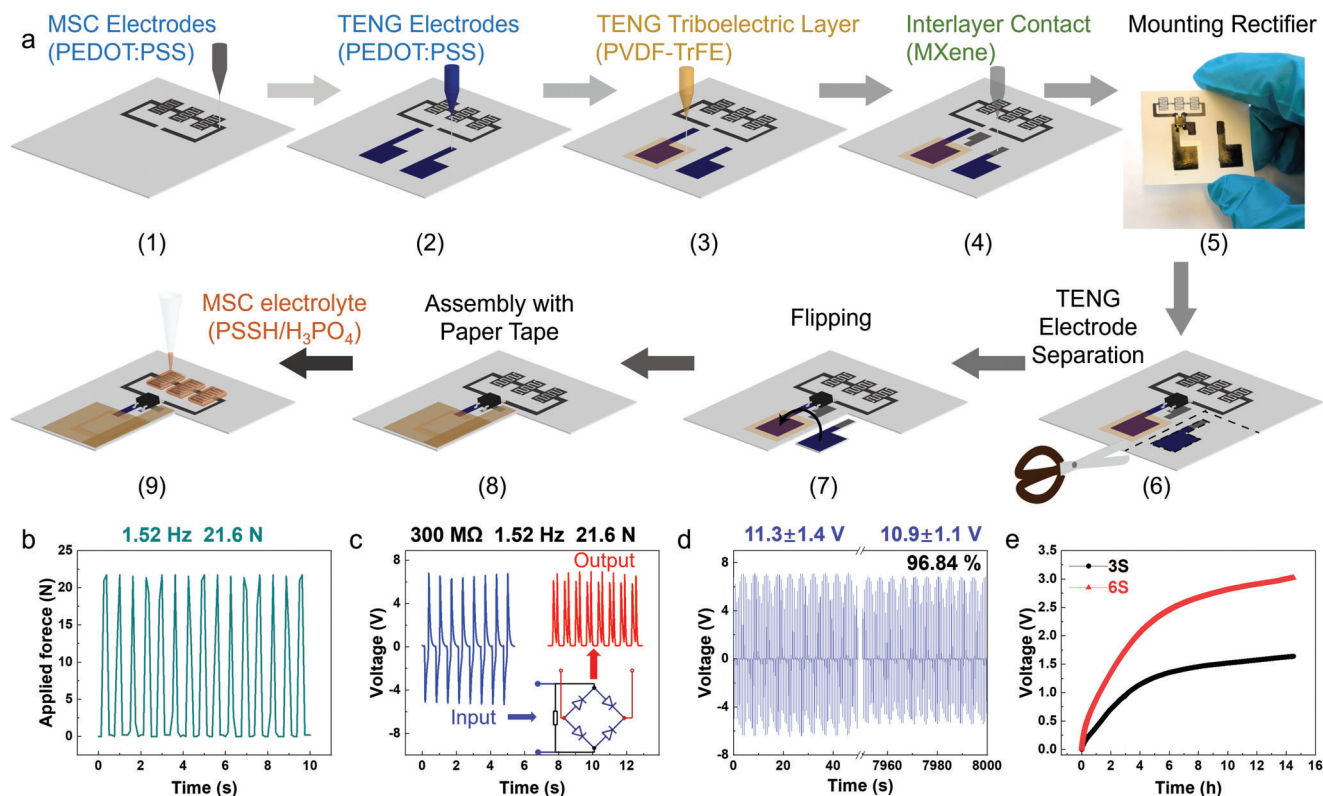
Figure 6. On-paper SCPSs. a) Schematic of the monolithic fabrication process. b) Applied force on the TENGs. c) Output voltage (with a load resistance of 300 MΩ) of a TENG before (blue) and after (red) the bridge rectifier. d) Cycling stability of the TENG in a SCPS under ≈12 000 continuous press-release cycles within 8000 s. e) Charging curves of the 3S and 6S MSC arrays in two SCPSs through ≈79 000 cycles of pressing and releasing the TENGs within 14.5 h.

(Figure 4c) and 150 nW (Figure 5e), respectively, our SCPS may suit some low-power electronics such as the continuous working mode for quartz crystal oscillators (100 nW) or the intermittent working mode for electronic watches (1 µW) and RFID tags (10 µW).[37]

3. Conclusion

We have developed a monolithic process to almost fully print metal-free SCPSs on paper substrates with a miniaturized footprint area of ≈2 cm × 3 cm and thickness of ≈1 mm. Stabilized by a small amount of carbon quantum dots, highly reliable and conductive PEDOT:PSS inks have been formulated in mixed water/EG solvents. The outstanding conformability of PEDOT:PSS on paper surface allows facile printing of highly rough conductive electrodes that can play multiple roles in the SCPSs, including large-area electrodes for MSCs with high-rate capability (>1000 mV s^{-1}), interconnect, and effective triboelectric electrodes for the TENGs, to avoid using spacer to simplify the TENG structure and enhance the miniaturization of the entire SCPSs. The full printing and nearly monolithic process enables us to flexibly tailor the cell number in the MSC arrays to improve the rate capability (e.g., to 6000 mV s^{-1} for the 6-cell series-connected MSC array) and increase the efficiency in storing the instantaneous (pulse) electricity from the TENGs. After continuous press and release of the TENGs for

≈79 000 cycles, the 3-cell MSC array can be charged to 1.6 V while the 6-cell array to 3.0 V. Except for the use of one commercial (non-printed) rectifier component in the present process, the monolithic process has shown promise to fabricate fully metal-free on-paper SCPSs as a lightweight, thin, sustainable, eco-friendly, and low-cost power supply for emerging electronics.

4. Experimental Section

Materials: Poly(3,4-ethylenedioxythiophene):poly(styrenesulfonate) (PEDOT:PSS, 1.1 wt.% in water, 739 332), Poly(4-styrenesulfonic acid) solution (PSSH, Mw ≈ 75 000, 18 wt.% in H$_2$O, 561 223), phosphoric acid (H$_3$PO$_4$, ≥85 wt. % in H$_2$O, 695 017), lithium fluoride (LiF, 98%, 237 965), Ti$_3$AlC$_2$ MAX (≥90%, 636 967) were ordered from Sigma-Aldrich. Ethylene glycol (EG, ≥99.5%, 03750) was purchased from Fluka. Poly(vinylidene fluoride–trifluorethylene) (PVDF-TrFE, Piezotech FC20, 20 mol% TrFE content) was purchased from Piezotech. Dimethyl sulfoxide (DMSO, ≥99%, 1.16743) was purchased from Supelco. Acetone and hydrochloric acid (HCl, electrograde, 37%) were purchased from Sunchem AB. The substrate for all the SCPSs and the components is the commercial Korsnäs white paperboard.

Carbon Quantum Dots (CQD) Synthesis: CQDs were synthesized through microwave-assisted irradiation of urea and citric acid as carbon sources.[20] First, the equal mass of urea and citric acid were dissolved in deionized water at the concentration of 105 mg mL^{-1}, followed by irradiation in a microwave oven at 800 W for up to 5 min. Then, after solvent

**ADVANCED
SCIENCE NEWS**

www.advancedsciencenews.com

**ADVANCED
FUNCTIONAL
MATERIALS**

www.afm-journal.de

evaporation, the black mass was scraped off the container walls and redispersed in deionized water at a concentration of 17 mg mL^{-1}.

MXene Ink Synthesis: Ti$_3$C$_2$T$_x$ MXene was synthesized through the minimal intensive layer delamination method according to previously published literature.[38] Briefly, 0.96 g of LiF was added to 12 mL of 9 M HCl and stirred for 5 min as an etchant. Then, 0.6 g of Ti$_3$AlC$_2$ MAX powder was gradually added to the above etchant over the course of 5 min and continuously stirred for 24 h at 35 °C. The acidic mixture was washed with deionized (DI) water via centrifuge at 3500 rpm for 5 min for several cycles until a pH 6 (according to the pH value of DI water in the lab) of the supernatant was achieved. The product was redispersed in DI water and centrifuged at 3500 rpm for 2 min to remove the non-etched Ti$_3$AlC$_2$ (sediment part). The dark supernatant was centrifuged at 1000 rpm for 1 h to acquire a stable of Ti$_3$C$_2$T$_x$ flakes. To dry a certain volume of Ti$_3$C$_2$T$_x$ dispersion and weigh the dried mass, the concentration was calculated. The final concentration of MXene ink is adjusted to 36 mg mL^{-1} by adding or removing DI water. The MXene ink was sealed and stored at 4 °C.

Poly(3,4-ethylenedioxythiophene):Poly(styrenesulfonate) (PEDOT:PSS) Ink Formulation: First, 0.8 mL of PEDOT:PSS solution was mixed with the 0.2 mL of EG solution and stirred for 30 min to obtain the PEDOT:PSS/EG ink. Then, 9 µL of CQDs (17 mg mL^{-1} in water) was dispersed in the 1 mL PEDOT:PSS/EG ink, sonicated for 30 min and stirred overnight. Roughly, the PEDOT:PSS/CQDs/EG ink comprises 8.71 mg mL^{-1} PEDOT:PSS, and 0.15 mg mL^{-1} CQDs. The zeta potential and particle size distribution of the diluted inks were measured by DLS meter (Zetasizer Nano-ZS ZEN 3600, Malvern Instruments, UK). The concentration of diluted PEDOT:PSS/CQDs/EG and PEDOT:PSS/EG solution for DLS is shown in Table S4 (Supporting Information).

MSC Fabrication: PEDOT:PSS/CQDs/EG ink was printed on the paper substrate using a Felix pro2 printer (FELIXprinters, Netherlands) with the adaptation of a ViscoTec printhead (vipro-HEAD 3/3, ViscoTec, Germany). The direct writing process of the Felix pro2 printer was controlled through G code commands by an open-source software Repetier-Host from FE-LIXPrinters. The printed interdigital electrodes naturally dried in the air overnight. Before electrochemical characterization, each MSC was drop cast with 20 µL of PSSH/H$_3$PO$_4$ (25:7, v/v) mixture electrolyte. The diluted conductive silver paste (AGG3790 and AGG3791, Agar Scientific Ltd., UK) was painted on the leads of the MSCs for external connection contacts. The MSCs or MSC arrays were loaded on a probe station (Signatone S1160 probe station equipped with S-725 micropositioners, Signatone Corporation, USA) connected with Gamry Interface 1010E potentiostat (Gamry Instruments Inc., USA) for electrochemical characterization. Cyclic voltammetry (CV), galvanostatic charge–discharge (GCD), and electrochemical impedance spectroscopy (EIS) were performed in a two-electrode system.

TENG Fabrication: The pair of upper and lower TENG electrodes, including the square (1.1 cm × 1.1 cm) charge collectors and the rectangle (3 cm × 0.3 cm) leads, were printed on the paper substrate with the PEDOT:PSS ink for three passes via the BIOprinter (FELIXprinters, Netherlands) controlled by G code commands. After drying at 60 °C in an oven overnight, the PEDOT:PSS electrodes were loaded back onto the BIOprinter to print the PVDF-TrFE triboelectric layer (1.6 cm×1.6 cm) to cover the square charge collector area of the lower PEDOT:PSS electrodes. The PVDF-TrFE inks comprise 10 wt.% PVDF-TrFE in the mixture solvent of DMSO/acetone (55:45, v/v). The printed PVDF-TrFE film was dried at 70 °C on a hotplate in fume hood, followed by annealing at 130 °C in an oven for 4 h. To assemble a TENG, the upper PEDOT:PSS electrode (without PVDF-TrFE film) was separated and aligned to the bottom electrode (with PVDF-TrFE film), and finally, the two electrodes were fixed/assembled with a paper-based tape (Tesa packing tape ECO FSC). The leads of the PEDOT:PSS electrodes were connected with Al/paper-based tape with diluted conductive silver paste for external electrical connection. For the mechanic energy harvesting tests, the force was applied through a LinMot linear motor (DM01-23×80F-HP-R-100) controlled by LinMot Talk software onto the TENG region and monitored with a force sensor (FlexiForce B201-Model), whose working diameter is 1 cm. The applied force and frequency were adjusted by the motor motion distance and motion speed. The output voltage and current were measured with a Gamry Interface 1010E potentiostat.

Monolithic Fabrication of the SCPSs: Following Figure 6a, the electrodes and interconnect for the MSC array and the TENG, the triboelectric layer of the TENG, and the interlayer contacts were printed on the same paper substrate with the PEDOT:PSS (1 pass for MSC electrodes and 3 passes for TENG electrodes and interconnect), PVDF-TrFE, and MXene (≈36 mg mL^{-1} in DI water) inks, respectively. After drying, a commercial bridge rectifier (751-4458, 6.7 mm × 4.7 mm × 2.6 mm containing pins, DiodesZetex, RS components Ltd.) was mounted with a double-sided tape onto the paper substrate to connect the TENG and MSC array. To enhance the conductivity, extra MXene ink was added to the contact areas and dried at 60 °C for 30 min. The upper electrode of TENG (without PVDF-TrFE film) was cut out and assembled via a paper tape with the lower electrode to form the complete TENG, as described in the TENG fabrication section. Finally, each MSC was drop cast with 20 µL PSSH/H$_3$PO$_4$ electrolyte to complete the fabrication of the SCPSs. A dovetail clip was used to fix the bridge rectifier to avoid detaching from the paper substrate during the cyclic press release applied by the motor. The charging voltage of the MSC array was monitored with a Gamry Interface 1010E potentiostat.

Statistical Analysis: Sample size (n = 3) was applied to the zeta potential, thickness, and sheet resistance measurements, and the data was presented in the form of mean ± standard deviation.

Supporting Information

Supporting Information is available from the Wiley Online Library or from the author.

Conflict of Interest

The authors declare no conflict of interest.

Data Availability Statement

The data that support the findings of this study are available from the corresponding author upon reasonable request.

[1] R. Y. Liu, Z. L. Wang, K. Fukuda, T. Someya, *Nat. Rev. Mater.* **2022**, *7*, 870.

[2] A. Petritz, E. Karner-Petritz, T. Uemura, P. Schaffner, T. Araki, B. Stadlober, T. Sekitani, *Nat. Commun.* **2021**, *12*, 2399.

[3] X. Pu, Z. L. Wang, *Chem. Sci.* **2020**, *12*, 34.

[4] P. P. Zhang, F. X. Wang, M. H. Yu, X. D. Zhuang, X. L. Feng, *Chem. Soc. Rev.* **2018**, *47*, 7426.

[5] N. Sun, Z. Wen, F. P. Zhao, Y. Q. Yang, H. Y. Shao, C. J. Zhou, Q. Q. Shen, K. Feng, M. F. Peng, Y. G. Li, X. H. Sun, *Nano Energy* **2017**, *38*, 210.

[6] Y. Gao, M. Rezaie, S. Choi, *Nano Energy* **2022**, *104*, 107923.

[7] W. T. Ma, M. Q. Zhang, W. Yan, J. B. Zhu, J. Z. Liu, W. X. Song, *Nano Energy* **2022**, *101*, 107601.

[8] H. Y. Guo, M. H. Yeh, Y. L. Zi, Z. Wen, J. Chen, G. L. Lin, C. G. Hu, Z. L. Wang, *ACS Nano* **2017**, *11*, 4475.

[9] H. Y. Guo, M. H. Yeh, Y. C. Lai, Y. L. Zi, C. S. Wu, Z. Wen, C. G. Hu, Z. L. Wang, *ACS Nano* **2016**, *10*, 10580.

[10] Z. F. Cong, W. B. Guo, Z. H. Guo, Y. H. Chen, M. M. Liu, T. T. Hou, X. Pu, W. G. Hu, Z. L. Wang, *ACS Nano* **2020**, *14*, 5590.

[11] S. L. Zhang, Q. Jiang, Z. Y. Wu, W. B. Ding, L. Zhang, H. N. Alshareef, Z. L. Wang, *Adv. Energy Mater.* **2019**, *9*, 1900152.

[12] J. Luo, W. Gao, Z. L. Wang, *Adv. Mater.* **2021**, *33*, 2004178.

[13] R. Walden, C. Kumar, D. M. Mulvihill, S. C. Pillai, *Chem. Eng. J. Adv.* **2022**, *9*, 100237.

[14] J. J. Luo, Z. L. Wang, *Ecomat* **2020**, *2*, e12059.

[15] C. Wu, A. C. Wang, W. Ding, H. Guo, Z. L. Wang, *Adv. Energy Mater.* **2019**, *9*, 1802906.

[16] J. Wang, Z. Wen, Y. Zi, P. Zhou, J. Lin, H. Guo, Y. Xu, Z. L. Wang, *Adv. Funct. Mater.* **2016**, *26*, 1070.

[17] B. Y. Ouyang, C. W. Chi, F. C. Chen, Q. F. Xi, Y. Yang, *Adv. Funct. Mater.* **2005**, *15*, 203.

[18] X. Fan, W. Nie, H. Tsai, N. Wang, H. Huang, Y. Cheng, R. Wen, L. Ma, F. Yan, Y. Xia, *Adv. Sci.* **2019**, *6*, 1900813.

[19] Z. Li, V. Ruiz, V. Mishukova, Q. Wan, H. Liu, H. Xue, Y. Gao, G. Cao, Y. Li, X. Zhuang, J. Weissenrieder, S. Cheng, J. Li, *Adv. Funct. Mater.* **2022**, *32*, 2108773.

[20] R. Seedad, S. khuthinakhun, N. Ratanawimarnwong, P. Jittangprasert, T. Mantim, K. Songsrirote, *New J. Chem.* **2021**, *45*, 22424.

[21] M. Saadi, A. Maguire, N. T. Pottackal, M. S. H. Thakur, M. M. Ikram, A. J. Hart, P. M. Ajayan, M. M. Rahman, *Adv. Mater.* **2022**, *34*, 2108855.

[22] S. Sollami Delekta, M. M. Laurila, M. Mantysalo, J. Li, *Nano-Micro Lett.* **2020**, *12*, 40.

[23] G. B. Min, Y. Xu, P. Cochran, N. Gadegaard, D. M. Mulvihill, R. Dahiya, *Nano Energy* **2021**, *83*, 105829.

[24] M. L. Seol, S. H. Lee, J. W. Han, D. Kim, G. H. Cho, Y. K. Choi, *Nano Energy* **2015**, *17*, 63.

[25] I. W. Tcho, W. G. Kim, S. B. Jeon, S. J. Park, B. J. Lee, H. K. Bae, D. Kim, Y. K. Choi, *Nano Energy* **2017**, *42*, 34.

[26] P. Pandey, D. H. Jung, G. J. Choi, M. K. Seo, S. Lee, J. M. Kim, I. Park, J. I. Sohn, *Nano Energy* **2023**, *107*, 108134.

[27] S. Potu, M. Navaneeth, R. K. Rajaboina, B. Gollapelli, J. Vallamkondu, S. Mishra, H. Divi, A. Babu, K. U. Kumar, P. Kodali, *ACS Appl. Energy Mater.* **2022**, *5*, 13702.

[28] X. S. Zhang, M. D. Han, R. X. Wang, F. Y. Zhu, Z. H. Li, W. Wang, H. X. Zhang, *Nano Lett.* **2013**, *13*, 1168.

[29] J. Q. Xiong, P. Cui, X. L. Chen, J. X. Wang, K. Parida, M. F. Lin, P. S. Lee, *Nat. Commun.* **2018**, *9*, 4280.

[30] R. A. Whiter, C. Boughey, M. Smith, S. Kar-Narayan, *Energy Technol.* **2018**, *6*, 928.

[31] H. Varghese, A. Chandran, *Sustainable Energy Fuels* **2021**, *5*, 5287.

[32] C. R. Qin, A. Lu, *Carbohydr. Polym.* **2021**, *274*, 118667.

[33] X. X. Shi, S. Chen, H. L. Zhang, J. X. Jiang, Z. Q. Ma, S. Q. Gong, *ACS Sustainable Chem. Eng.* **2019**, *7*, 18657.

[34] J. J. Luo, F. R. Fan, T. Jiang, Z. W. Wang, W. Tang, C. P. Zhang, M. M. Liu, G. Z. Cao, Z. L. Wang, *Nano Res.* **2015**, *8*, 3934.

[35] X. Y. Gao, Y. Z. Zhang, S. K. Yin, Y. Q. Mao, J. Z. Gui, J. X. Li, Y. F. Zhao, C. L. Sun, S. S. Guo, *Adv. Funct. Mater.* **2022**, *32*, 2204833.

[36] C. Zhang, Z. X. Peng, C. L. Huang, B. W. Zhang, C. Xing, H. M. Chen, H. Y. Cheng, J. Wang, S. L. Tang, *Nano Energy* **2021**, *81*, 105609.

[37] P. P. Zhang, F. X. Wang, S. Yang, G. Wang, M. H. Yu, X. L. Feng, *Energy Storage Mater.* **2020**, *28*, 160.

[38] M. Alhabeb, K. Maleski, B. Anasori, P. Lelyukh, L. Clark, S. Sin, Y. Gogotsi, *Chem. Mater.* **2017**, *29*, 7633.